

Hierarchical Visualization of Materials Space with Graph Convolutional Neural Networks

Tian Xie¹ and Jeffrey C. Grossman¹

Department of Materials Science and Engineering, Massachusetts Institute of Technology, Cambridge, Massachusetts 02139, United States

(Dated: 14 December 2024)

The combination of high throughput computation and machine learning has led to a new paradigm in materials design by allowing for the direct screening of vast portions of structural, chemical, and property space. The use of these powerful techniques leads to the generation of enormous amounts of data, which in turn calls for new techniques to efficiently explore and visualize the materials space to help identify underlying patterns. In this work, we develop a unified framework to hierarchically visualize the compositional and structural similarities between materials in an arbitrary material space. We demonstrate the potential for such a visualization approach by showing that patterns emerge automatically that reflect similarities at different scales in three representative classes of materials: perovskites, elemental boron, and general inorganic crystals, covering material spaces of different compositions, structures, and both. For perovskites, elemental similarities are learned that reflects multiple aspects of atom properties. For elemental boron, structural motifs emerge automatically showing characteristic boron local environments. For inorganic crystals, the similarity and stability of local coordination environments are shown combining different center and neighbor atoms. The method could help transition to a data-centered exploration of materials space in automated materials design.

I. INTRODUCTION

Efficient exploration of the materials space has been central to material discovery as a result of the limited experimental and computational resources compared with its vast size. Often compositional or structural patterns are sought from past experiences that might guide the design of new materials, improving the efficiency of material exploration^{1–5}. Emerging high-throughput computation and machine learning techniques directly screen large amounts of candidate materials for specific applications^{6–12}, which enables fast and direct exploration of the material space. However, the large quantities of material data generated makes the discovery of patterns challenging with traditional, human-centered approaches. Instead, an automated, data-centered method to visualize and understand a given materials design phase space is needed in order to improve the efficiency of exploration. Early efforts usually rely on human designed similarity metrics that are based on substitution probability¹³ or local descriptors¹⁴. Recently, we¹⁵ and Schutt et al.¹⁶ concurrently developed graph-based representations of solid materials, providing a general framework to predict material properties accurately without any human designed features. This framework provides a natural way to represent any material in the vector space, which allows the visualization of material space from learned models. For instance, several works have investigated the ideas of visualizing atom energies^{15,17,18} and elemental similarities^{19,20}.

In this work, we develop a framework that unify these ideas to hierarchically visualize the compositional and structural similarities between materials in an arbitrary material space. The method is based on a variant of our previously developed crystal graph convolutional neural networks (CGCNN) framework¹⁵, but it is designed to

focus on presenting the similarities between materials at different scales, including elemental similarities, local environment similarities, and local energies. We apply this approach to visualize three material spaces: perovskites, elemental boron, and general inorganic crystals, covering material spaces of different compositions, different structures, and both, respectively. We show that in all three cases pattern emerges automatically that can aid in the design of new materials.

II. METHODS

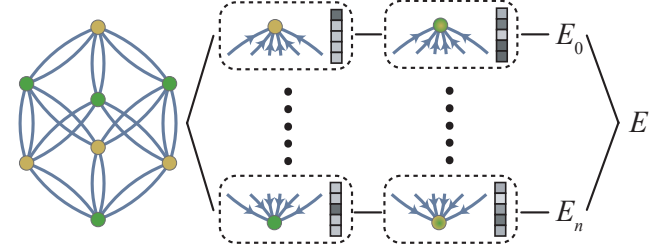


FIG. 1. The structure of the crystal graph convolutional neural networks.

To visualize the crystal space at different scales, we design a variant of CGCNN¹⁵ that has meaningful interpretation at different layers of the neural network. The learned CGCNN network provides a vector representation of the local environments in each crystal that only depends on its composition and structure without any human designed features, enabling us to explore the materials space hierarchically.

We first represent the crystal structure with a multi-graph \mathcal{G} that encodes the connectivity of atoms in the

crystal. Each atom is represented by a node i in \mathcal{G} which stores a vector \mathbf{v}_i corresponding to the element type of the atom. To avoid introducing any human bias, we set \mathbf{v}_i to be a random 64 dimensional vector for each element and allow it to evolve during the training process. Then, we search for the 12 nearest neighbors for each atom and introduce an edge $(i, j)_k$ between the center node i and neighbor j . The subscript k indicates that there can be multiple edges between the same end nodes as a result of the periodicity of the crystal. The edge $(i, j)_k$ stores a vector $\mathbf{u}_{(i,j)_k}$ whose t th element depends on the distance between i and j by,

$$\mathbf{u}_{(i,j)_k}[t] = \exp(-(d_{(i,j)_k} - \mu_t)^2/\sigma^2) \quad (1)$$

where $\mu_t = t \cdot 0.2 \text{ \AA}$ for $t = 0, 1, \dots, 40$ and $\sigma = 0.2 \text{ \AA}$.

In graph \mathcal{G} , each atom i is initialized by a vector \mathbf{v}_i whose value solely depends on the element type of atom i . We call this iteration 0 where

$$\mathbf{v}_i^{(0)} = \mathbf{v}_i \quad (2)$$

Then, we perform convolution operations on the multi-graph \mathcal{G} with the convolution function designed in Ref.¹⁵ which allows atom i to interact with its neighbors iteratively. In iteration t , we first concatenate neighbor vectors $\mathbf{z}_{(i,j)_k}^{(t-1)} = \mathbf{v}_i^{(t-1)} \oplus \mathbf{v}_j^{(t-1)} \oplus \mathbf{u}_{(i,j)_k}$, and then perform the convolution by,

$$\begin{aligned} \mathbf{v}_i^{(t)} = & \mathbf{v}_i^{(t-1)} + \sum_{j,k} \sigma(\mathbf{z}_{(i,j)_k}^{(t-1)} \mathbf{W}_f^{(t-1)} + \mathbf{b}_f^{(t-1)}) \\ & \odot g(\mathbf{z}_{(i,j)_k}^{(t-1)} \mathbf{W}_s^{(t-1)} + \mathbf{b}_s^{(t-1)}) \quad (3) \end{aligned}$$

where \odot denotes element-wise multiplication, σ denotes a sigmoid function, and g denotes any non-linear activation function, and \mathbf{W} and \mathbf{b} denotes weights and biases in the neural network, respectively. During these convolution operations, $\mathbf{v}_i^{(t)}$ forms a series of representations of the local environments of atom i at different scales.

After K iterations, we perform a linear transformation to map $\mathbf{v}_i^{(K)}$ to a scalar E_i ,

$$E_i = \mathbf{v}_i^{(K)} \mathbf{W}_l + b_l \quad (4)$$

and then use a normalized sum pooling to predict the averaged total energy per atom of the crystal,

$$E = \frac{1}{n} \sum_i E_i \quad (5)$$

where n is the number of atoms in the crystal. This introduces a physically meaningful term E_i to represent the energy of the local chemical environment.

The model is trained by minimizing the squared error between predicted properties relative to the DFT calculated properties using backpropagation and stochastic gradient descent.

In this CGCNN model, each vector represents the local environment of each atom at different scales. Here, we focus three vectors that has the most representative physical interpretations.

1. *Element representation* $\mathbf{v}_i^{(0)}$ that depends completely on the type of element that atom i is composed of, describing the similarities between elements.
2. *Local environment representation* $\mathbf{v}_i^{(K)}$ that depends on atom i and its K th order neighbors, describing the similarities between local environments that combines the compositional and structural information.
3. *Local energy representation* E_i that describes the energy of atom i .

III. RESULTS AND DISCUSSIONS

To illustrate how this method can help visualize the compositional and structural aspects of the crystal space, we apply it to three datasets that representing different material spaces. 1) a group of perovskite crystals that share the same structure type but have different compositions; 2) different configurations of elemental boron that share the same composition but have different structures; and 3) inorganic crystals from the Materials Project²¹ that have both different compositions and different structures.

A. Perovskite: compositional space

First, we explore the compositional space of perovskites by visualizing the *element representations*. Perovskite is a crystal structure type with the form of ABC_3 as shown in Fig. 2(a). The dataset that we used includes 18,928 different perovskites where the elements A and B can be any nonradioactive metals and the element C can be one or several from O, N, S, and F. We trained our model to predict the energy above hull with 15,000 training data, and after hyperparameter optimization on 1,890 validation data, we achieve a prediction mean absolute error (MAE) of 0.042 eV/atom on 2,000 test data. The prediction performance is excellent and lower than several recent ML models such as those of Schmidt et al. (0.121 eV/atom)¹⁹ and Xie et al. (0.099 eV/atom)¹⁵.

In Fig. 2(b)(c), the element representation $\mathbf{v}_i^{(0)}$, a 64 dimensional vector, is visualized for every nonradioactive metal element after training with the perovskite dataset. Fig. 2(b) shows the projection of these element representations on a 2D plane using principal component analysis, where elements are colored according to their elemental groups. We can clearly see that similar elements are grouped together based on their stability in perovskite structures. For instance, alkali metals are grouped on the right of the plot due to their similar properties. The large alkaline earth metals (Ba, Se, and Ca) are grouped on the bottom, distinct from Mg and Be, because their larger radius stabilizes them in the perovskite structure.

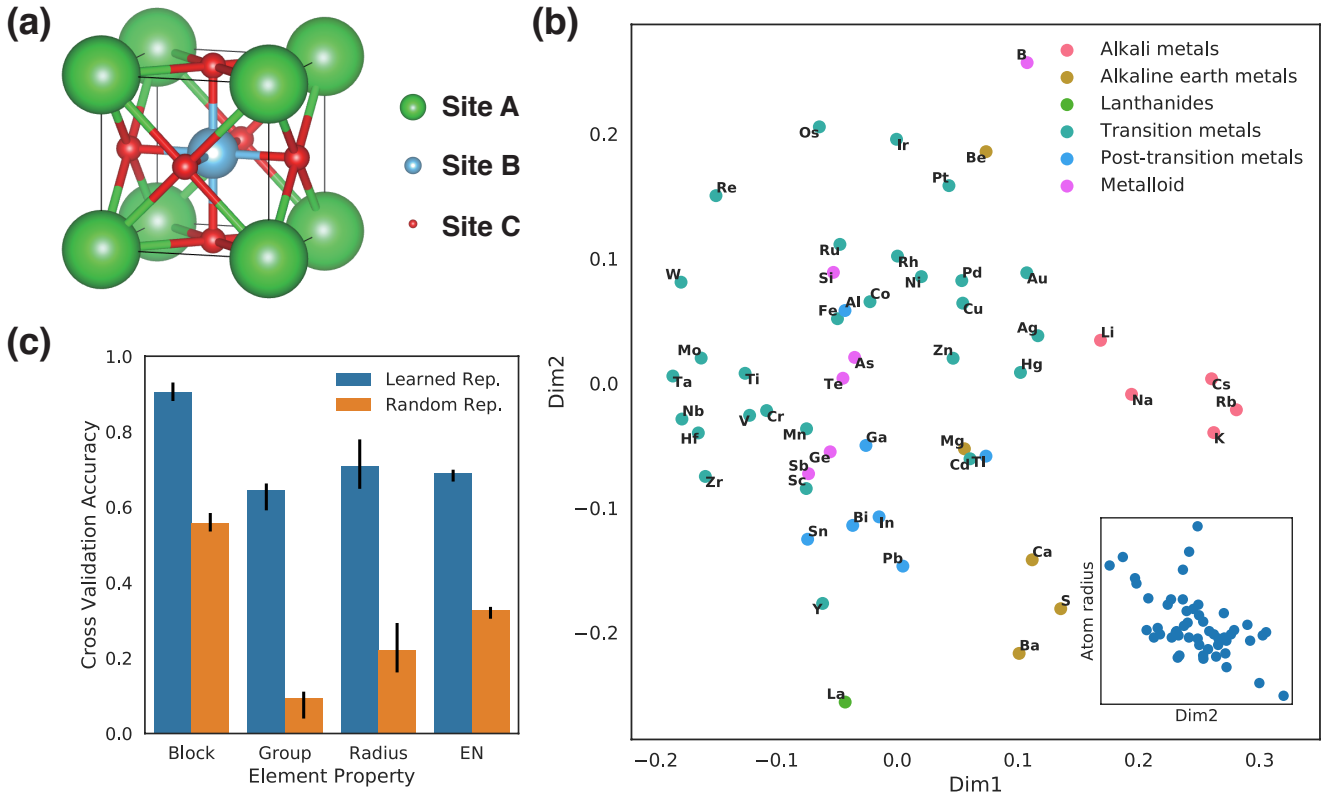


FIG. 2. Visualization of the element representations learned from the perovskite dataset. (a) The perovskite structure type. (b) Visualization of the two principal dimensions with principal component analysis. (c) Prediction performance of several atom properties using a linear model on the element representations.

On the left side are elements such as W, Mo, and Ta that favor octahedral coordinations due to their configuration of d electrons, which might be related to their extra stability in the B site¹⁵. Interestingly, we can also observe a trend of decreasing atom radius from the bottom of the plot to the top as shown in the insert of Fig. 2(b), except for the alkali metals as outliers. This indicates that CGCNN learns the atom radius as an important feature for perovskite stability. Recently, Schutt et al. also discovered similar grouping of elements with data from the Materials Project¹⁶. In general, these visualizations can help discover similarities between elements for designing novel perovskite structures.

However, these 2D plots only account for part of the 64-dimensional element representation vectors. To fully understand how element properties are learned by CGCNN, we use linear logistic regression (LR) models to predict the block type, group number, radius, and electronegativity of each element from their learned representation vectors. In Fig. 2(c), we show the 3-fold cross validation accuracy of the LR models and compare them with LR models learned from random representations, which helps to rule out the possibility that the predictions are caused by coincidences. We discover a significantly higher prediction accuracy of the learned representations

for all four properties, demonstrating that the element representations can reflect multiple aspects of element properties. For instance, the model predicts the block of the element with over 90% accuracy, and the same representation also predicts the group number, radius, and electronegativity with over 60% accuracy. This is surprising considering that there are 16 different elemental groups represented. It is worth noting that these representations are learned only from the perovskite structures and the total energy above hull, but they are in agreement with these empirical element properties reflecting decades of human chemical intuition.

B. Elemental boron: structural space

As a second example, we explore the structural space of elemental boron by visualizing the *local environment representations* and the corresponding *local energies*. Elemental boron has a number of complex crystal structures due to its unique, electron-deficient bonding nature^{17,23}. We use a dataset that includes 5038 distinct elemental boron structures and their total energies calculated using density functional theory¹⁷. We train our CGCNN model with 3038 structures, and perform hyperparam-

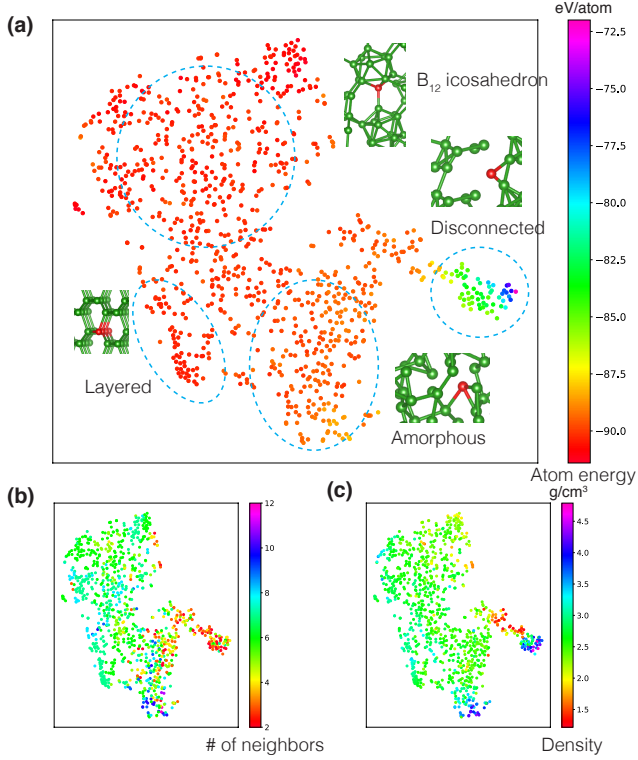


FIG. 3. Visualization of the local environment representations learned from the elemental boron dataset. The original 64D vectors are reduced to 2D with the t-distributed stochastic neighbor embedding algorithm. The color of each plot is coded with learned local energy (a), number of neighbors calculated by Pymatgen package²² (b), and density (c). Representative boron local environments are shown with the center atom colored in red.

eter optimization with 1000 validation structures. The MAE of predicted energy relative to DFT results on the remaining 1000 test structures is 0.085 eV/atom. The corresponding root-mean-square error (RMSE) is 0.126 eV/atom.

In Fig. 3, 1000 randomly sampled boron local environment representations are visualized in 2 dimensions using the t-distributed stochastic neighbor embedding (t-SNE) algorithm²⁴. We observe primarily four different regions of different boron local environments, and we discover a smooth transition of local energy, number of neighbor atoms, and the density between different regions. The disconnected region consists of boron atoms at the edge of boron clusters [Fig. S1(a-c)]. These atoms have very high local energies and lower number of neighbors, as to be expected, and their density varies depending on the distances between clusters. The amorphous region includes boron atoms in a relatively disordered local configuration, and their local energies are lower than the disconnected counterparts but higher than other other configurations [Fig. S1(d-f)]. We can see that the number of neighbors fluctuates drastically in these two regions due to the relatively disordered local structures. The lay-

ered region is composed of boron atoms in layered boron planes, where neighbors on one side are closely bonded and the neighbors on the other side are further away [Fig. S1(g-i)]. The B₁₂ icosahedron region includes boron local environments with the lowest local energy, which have a characteristic icosahedron structure [Fig. S1(j-l)]. The local environments in each region share common characteristics but are slightly different in detail. For instance, most boron atoms in the B₁₂ icosahedron region are in a slightly distorted icosahedron, and the local environments in Fig. S1(l) only have certain features of an icosahedron. Note that these representations are rather localized. The global structure of Fig. S1(c) is layered, but the representation of the highlighted atom at the edge is closer to the disconnected region locally.

Taken together, such a visualization approach provides a convenient way to explore complex boron configurations, enabling the identification of characteristic structures and systematic exploration of structural space.

C. Materials Project: compositional and structural space

As a third example of applying this approach, we explore the material space of crystals in the Materials Project dataset²¹, which includes both compositional and structural differences, by visualizing the *element representation*, *local environment representation*, and the *local energy representation*. The dataset includes 46744 materials that cover the majority of crystals from the Inorganic Crystal Structure Database²⁶, providing a good representation of known inorganic materials. After training with 28046 crystals and performing hyperparameter optimization with 9348 crystals, our model achieves MAE of predicted energy relative to DFT calculations on the 9348 test crystals of 0.042 eV/atom, slightly higher than the MAE of our previous work, 0.039 eV/atom, with a CGCNN structure focusing on prediction performance¹⁵.

In Fig. S2, the element representation of 89 elements learned from the dataset is shown using the same method as that used to generate Fig. 2(b). We observe similar grouping of elements from the same elemental groups, but the overall pattern differs since it reflect the stability of each element in general inorganic crystals rather than perovskites. For instance, the non-metal and halogen elements stand out because their properties deviates from other metallic elements.

To illustrate how the compositional and structural spaces can be explored simultaneously, we visualize the oxygen and sulfur coordination environments in the Materials Project dataset using the local environment representation and local energy. 1000 oxygen and 803 sulfur coordination environments are randomly selected and visualized using the t-SNE algorithm. As shown in Fig. 4(a), the oxygen coordination environments are clustered into 4 major groups. The upper right group has the center atom of non-metal elements like P, Al, Si, forming tetrahedron coordinations. The center atoms of the up-

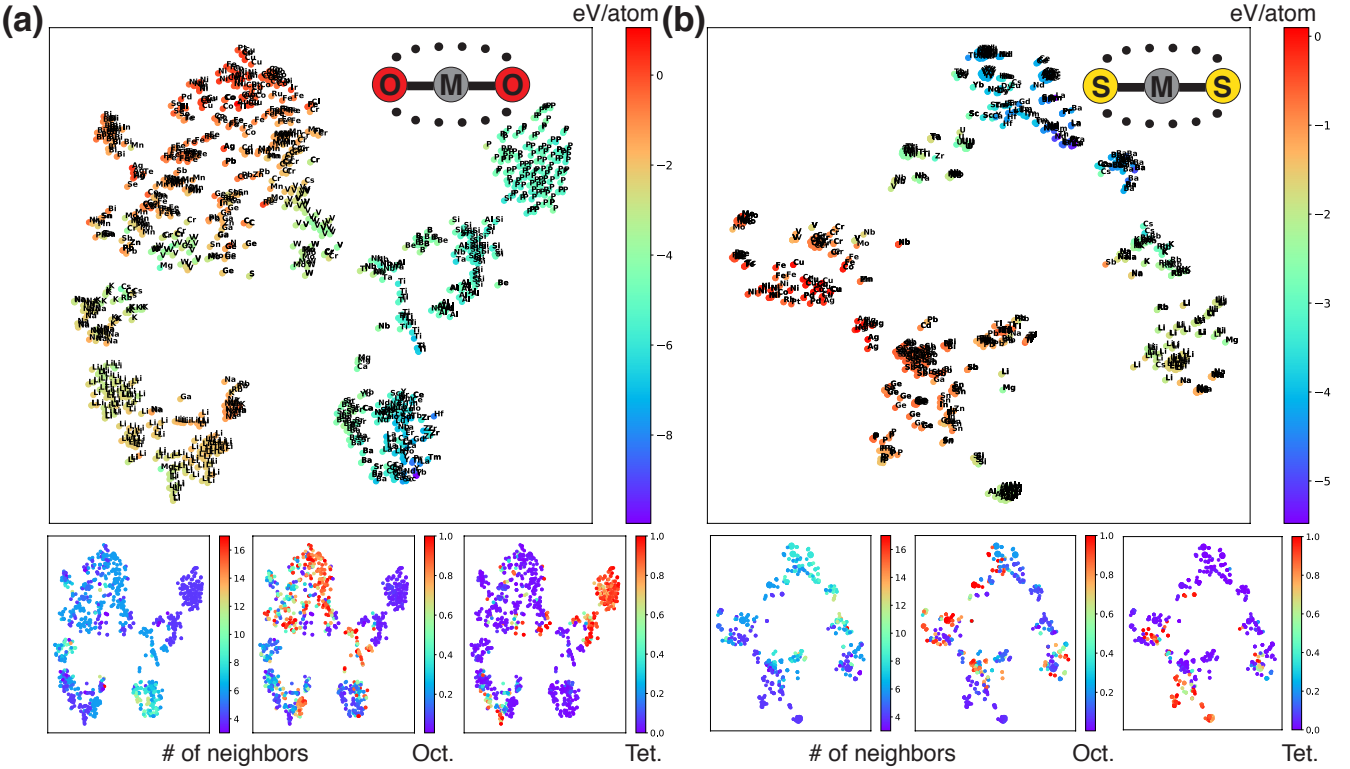


FIG. 4. Visualization of the local oxygen (a) and sulfur (b) coordination environments. The points are labelled according to the type of the center atoms in the coordination environments. The colors of the upper parts are coded with learned local energies, and the color of the lower parts are coded with number of neighbors²², octahedron order parameter, and tetrahedron order parameter²⁵.

per left environments are mostly transition metals, and they mostly form octahedron coordinations. The lower left group has center atoms of alkali metals, and the lower right group has those of alkaline earth metals and lanthanides which have larger radii and therefore higher coordination numbers. The sulfur coordination environment visualization [Fig. 4(b)] shares similar patterns due to the similarities between oxygen and sulfur, and a similar four-cluster structure can be observed. However, instead of non-metal elements, the lower center group has center atoms of metalloids like Ge, Sn, Sb, since these elements will be more stable in a sulfur vs. oxygen coordination environment.

The local energy of oxygen and sulfur coordination environments are determined by their relative stability to the pure elemental states since the model is trained using the formation energy data, which treats the pure elemental states as the reference energy states. In Fig. S3, we show the change of local energy of oxygen and sulfur local energies as a function of atomic number. We can clearly see that it follows a similar trend as the electronegativity of the elements: elements with lower electronegativity tend to have lower local energy and vice versa. This is because elements with lower electronegativity tends to give the oxygen and sulfur more electrons and thus form stronger bonds. The local energies of alkali metals are

slightly higher since they form weaker ionic bonds due to lower charges. Interestingly, the strong covalent bonds between oxygen and Al, Si, P, S forms a V-shaped curve in the figure, with Si-O environments having the lowest energy, contrasting the trend of electronegativity and sulfur coordination environments, whose local energies are dominated by the strength of ionic bonds. We also observe a larger span of local energies in oxygen coordination environments than their sulfur counterparts due to the stronger ionic interactions.

Inspired by these results, we visualize the averaged local energy of 734,077 distinct coordination environments in the Materials Project by combining different center and neighbor atoms in Fig. 5. This figure illustrates the stability of the local coordination environment while combining the corresponding center and neighbor elements. The diagonal line represents coordination environments made up with the same elements with local energy close to zero, which corresponds to elemental substances with zero formation energy. The coordination environments with lowest local energy consist of high valence metals and high electronegativity non-metals, which can be explained by the large cohesive energies due to strong ionic bonds. One abnormality is the stable Al-O, Si-O, P-O, S-O coordination environments, although this can be attributed to their strong covalent

bonds. We can also see that Tm-H coordination stands out as a stable hydrogen solid solution²⁷. It is worth noting that each local energy in Fig. 5 is the average of many coordination environments with different shape and outer layer chemistry, and we can obtain more information by using additional visualizations similar to Fig. 4.

IV. SUMMARY

In summary, we developed a unified approach to visualize the compositional and structural space of materials. The method provides hierarchical representations of the local environments at different scales, which enables a general framework to explore different material systems and measure material similarities. The insights gained from the visualizations could help to discover patterns from a large pool of candidate materials that may be impossible by human analysis, and provide guidance to the design of new materials. In addition to energies, this method can potentially be applied to other material properties for the exploration of novel functional materials.

- ¹G. Niu, X. Guo, and L. Wang, “Review of recent progress in chemical stability of perovskite solar cells,” *Journal of Materials Chemistry A* **3**, 8970–8980 (2015).
- ²H. J. Snaith, “Perovskites: the emergence of a new era for low-cost, high-efficiency solar cells,” *The Journal of Physical Chemistry Letters* **4**, 3623–3630 (2013).
- ³M. Xu, T. Liang, M. Shi, and H. Chen, “Graphene-like two-dimensional materials,” *Chemical reviews* **113**, 3766–3798 (2013).
- ⁴S. Z. Butler, S. M. Hollen, L. Cao, Y. Cui, J. A. Gupta, H. R. Gutiérrez, T. F. Heinz, S. S. Hong, J. Huang, A. F. Ismach, *et al.*, “Progress, challenges, and opportunities in two-dimensional materials beyond graphene,” *ACS nano* **7**, 2898–2926 (2013).
- ⁵O. Madelung, *Physics of III-V compounds* (J. Wiley, 1964).
- ⁶J. Greeley, T. F. Jaramillo, J. Bonde, I. Chorkendorff, and J. K. Nørskov, “Computational high-throughput screening of electrocatalytic materials for hydrogen evolution,” *Nature materials* **5**, 909 (2006).
- ⁷S. M. Senkan, “High-throughput screening of solid-state catalyst libraries,” *Nature* **394**, 350 (1998).
- ⁸R. Potyrailo, K. Rajan, K. Stoewe, I. Takeuchi, B. Chisholm, and H. Lam, “Combinatorial and high-throughput screening of materials libraries: review of state of the art,” *ACS combinatorial science* **13**, 579–633 (2011).
- ⁹S. Curtarolo, G. L. Hart, M. B. Nardelli, N. Mingo, S. Sanvito, and O. Levy, “The high-throughput highway to computational materials design,” *Nature materials* **12**, 191 (2013).
- ¹⁰G. Hautier, C. C. Fischer, A. Jain, T. Mueller, and G. Ceder, “Finding natures missing ternary oxide compounds using machine learning and density functional theory,” *Chemistry of Materials* **22**, 3762–3767 (2010).
- ¹¹R. Gómez-Bombarelli, J. Aguilera-Iparraguirre, T. D. Hirzel, D. Duvenaud, D. Maclaurin, M. A. Blood-Forsythe, H. S. Chae, M. Einzinger, D.-G. Ha, T. Wu, *et al.*, “Design of efficient molecular organic light-emitting diodes by a high-throughput virtual screening and experimental approach,” *Nature materials* **15**, 1120 (2016).
- ¹²P. Raccuglia, K. C. Elbert, P. D. Adler, C. Falk, M. B. Wenny, A. Mollo, M. Zeller, S. A. Friedler, J. Schrier, and A. J. Norquist, “Machine-learning-assisted materials discovery using failed experiments,” *Nature* **533**, 73 (2016).
- ¹³L. Yang and G. Ceder, “Data-mined similarity function between material compositions,” *Physical Review B* **88**, 224107 (2013).
- ¹⁴S. De, A. P. Bartók, G. Csányi, and M. Ceriotti, “Comparing molecules and solids across structural and alchemical space,” *Physical Chemistry Chemical Physics* **18**, 13754–13769 (2016).
- ¹⁵T. Xie and J. C. Grossman, “Crystal graph convolutional neural networks for an accurate and interpretable prediction of material properties,” *Physical Review Letters* **120**, 145301 (2018).
- ¹⁶K. T. Schütt, H. E. Sauceda, P.-J. Kindermans, A. Tkatchenko, and K.-R. Müller, “Schnet—a deep learning architecture for molecules and materials,” *The Journal of Chemical Physics* **148**, 241722 (2018).
- ¹⁷V. L. Deringer, C. J. Pickard, and G. Csányi, “Data-driven learning of total and local energies in elemental boron,” *Physical review letters* **120**, 156001 (2018).
- ¹⁸K. T. Schütt, F. Arbabzadah, S. Chmiela, K. R. Müller, and A. Tkatchenko, “Quantum-chemical insights from deep tensor neural networks,” *Nature communications* **8**, 13890 (2017).
- ¹⁹J. Schmidt, J. Shi, P. Borlido, L. Chen, S. Botti, and M. A. Marques, “Predicting the thermodynamic stability of solids combining density functional theory and machine learning,” *Chemistry of Materials* **29**, 5090–5103 (2017).
- ²⁰Q. Zhou, P. Tang, S. Liu, J. Pan, Q. Yan, and S.-C. Zhang, “Learning atoms for materials discovery,” *Proceedings of the National Academy of Sciences* , 201801181 (2018).
- ²¹A. Jain, S. P. Ong, G. Hautier, W. Chen, W. D. Richards, S. Dacek, S. Cholia, D. Gunter, D. Skinner, G. Ceder, and K. a. Persson, “The Materials Project: A materials genome approach to accelerating materials innovation,” *APL Materials* **1**, 011002 (2013).
- ²²S. P. Ong, W. D. Richards, A. Jain, G. Hautier, M. Kocher, S. Cholia, D. Gunter, V. L. Chevrier, K. A. Persson, and G. Ceder, “Python materials genomics (pymatgen): A robust, open-source python library for materials analysis,” *Computational Materials Science* **68**, 314 – 319 (2013).
- ²³T. Ogitsu, E. Schwegler, and G. Galli, “ β -rhombohedral boron: at the crossroads of the chemistry of boron and the physics of frustration,” *Chemical reviews* **113**, 3425–3449 (2013).
- ²⁴L. v. d. Maaten and G. Hinton, “Visualizing data using t-sne,” *Journal of machine learning research* **9**, 2579–2605 (2008).
- ²⁵N. E. R. Zimmermann, M. K. Horton, A. Jain, and M. Haranczyk, “Assessing local structure motifs using order parameters for motif recognition, interstitial identification, and diffusion path characterization,” *Frontiers in Materials* **4**, 34 (2017).
- ²⁶M. Hellenbrandt, “The inorganic crystal structure database (icsd) present and future,” *Crystallography Reviews* **10**, 17–22 (2004).
- ²⁷J. Bonnet and J. Daou, “Study of the hydrogen solid solution in thulium,” *Journal of Physics and Chemistry of Solids* **40**, 421–425 (1979).
- ²⁸B. Cordero, V. Gómez, A. E. Platero-Prats, M. Revés, J. Echeverría, E. Cremades, F. Barragán, and S. Alvarez, “Covalent radii revisited,” *Dalton Transactions* , 2832–2838 (2008).
- ²⁹Mentel, “mendeleev – a python resource for properties of chemical elements, ions and isotopes,” .

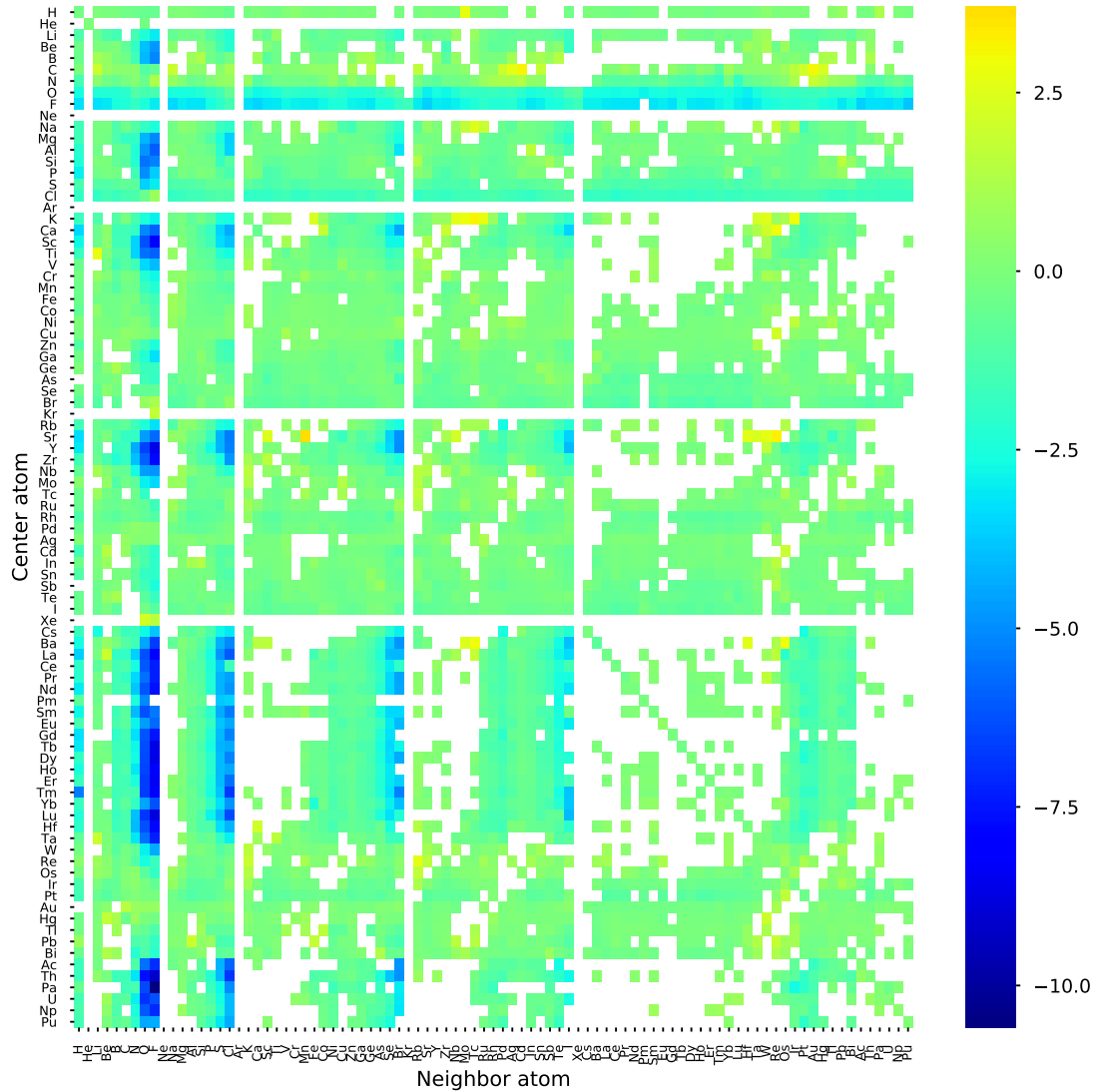


FIG. 5. The averaged local energy of 734,077 distinct coordination environments in the Materials Project dataset. The color is coded with the average of learned local energies while having the corresponding elements as the center atom and the first neighbor atom. White is used when no such coordination environment exists in the dataset.

Supplemental Materials: Hierarchical Visualization of Materials Space with Graph Convolutional Neural Networks

V. SUPPLEMENTARY METHODS

A. Logistic Regression Models

In the perovskite dataset, we use logistic regression models to predict four different elemental properties. We treat all four predictions as classification problem for consistency, although some of the properties have continuous values. We summarized the categories of each elemental properties in Table S2.

VI. SUPPLEMENTARY TABLES

TABLE S1. Hyperparameters selected for each dataset.

Dataset	# of convolutional layers	Length of representation $v_i^{(t)}$	learning rate
Perovskites	4	64	0.005
Elemental B	4	64	0.005
Materials Project	4	64	0.005

TABLE S2. The categories of each elemental property logistic regression models.

Elemental property	# of categories	Categories
Block	3	s, p, d
Group	16	1, 2, ..., 16
Radius (Å) ²⁸	5	[83, 116), [116, 148), [148, 180), [180, 212), [212, 244)
Electronegativity ²⁹	5	[0.788, 1.112), [1.112, 1.434), [1.434, 1.756), [1.756, 2.078), [2.078, 2.4)

VII. SUPPLEMENTARY FIGURES

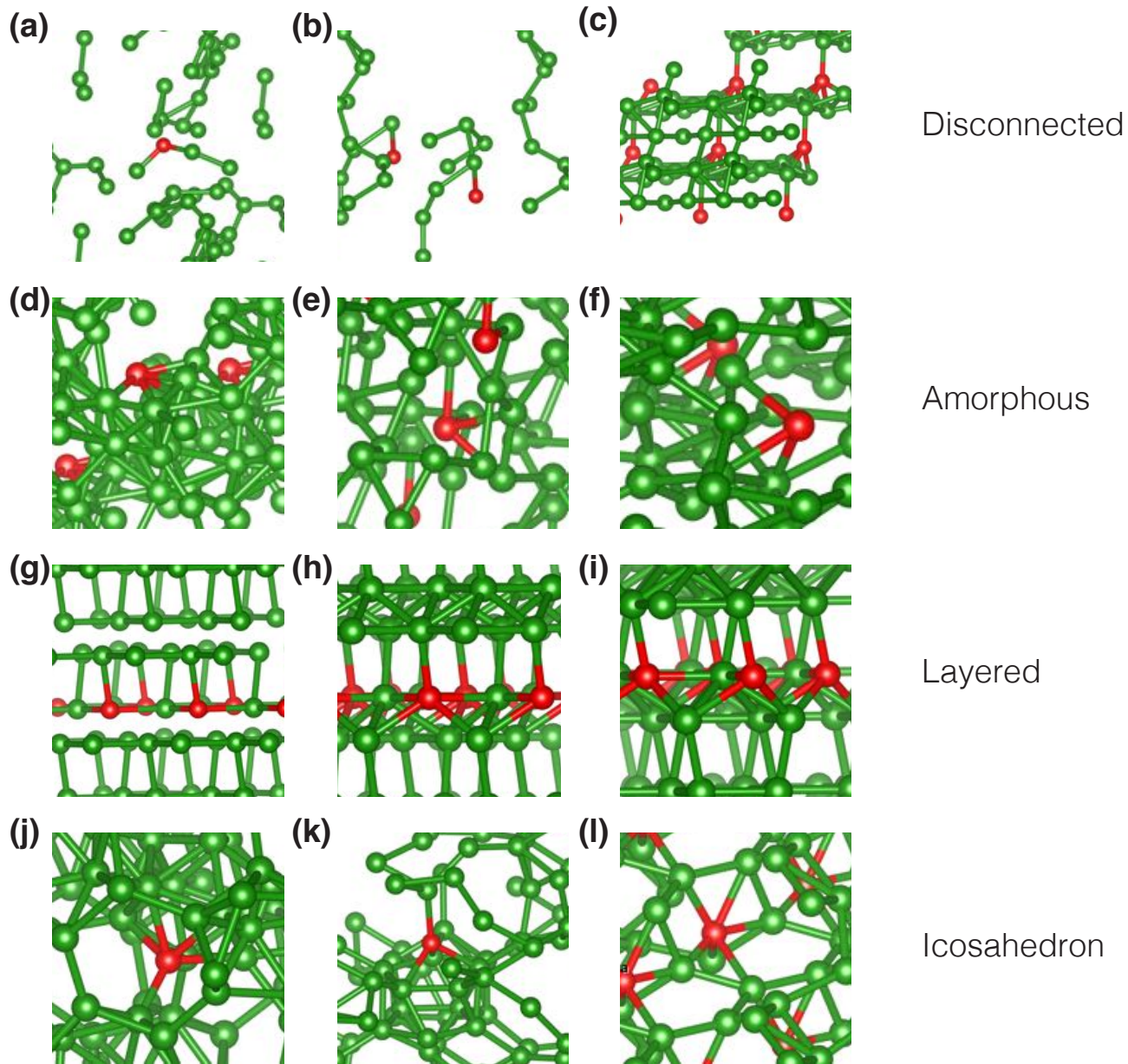


FIG. S1. Example local environments of elemental boron in the four regions: (a-c) disconnected, (d-f) amorphous, (h-i) layered, and (j-l) icosahedron.

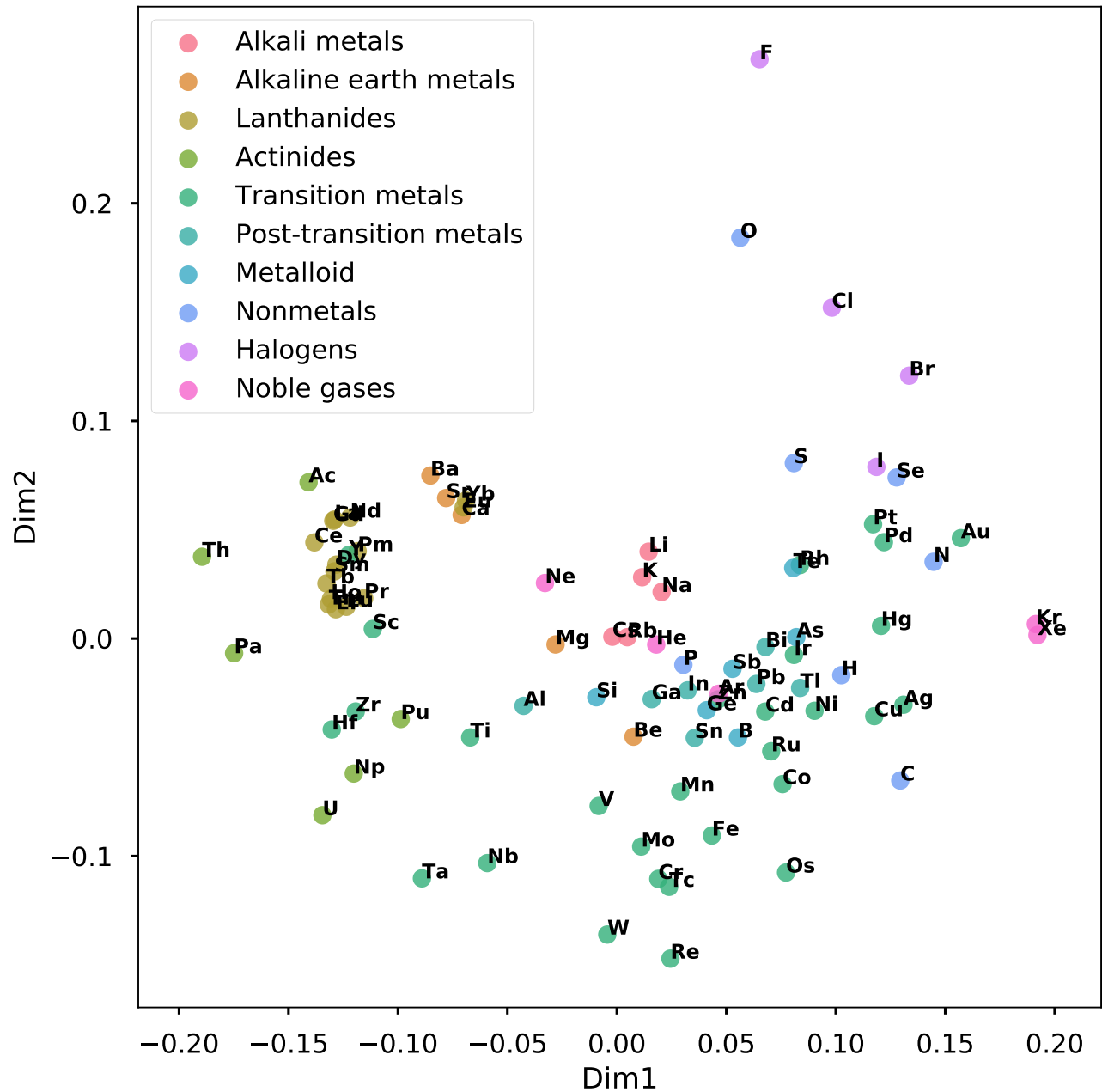


FIG. S2. Visualization of the two principal dimensions of the element representations learned from the Materials Project dataset using principal component analysis.

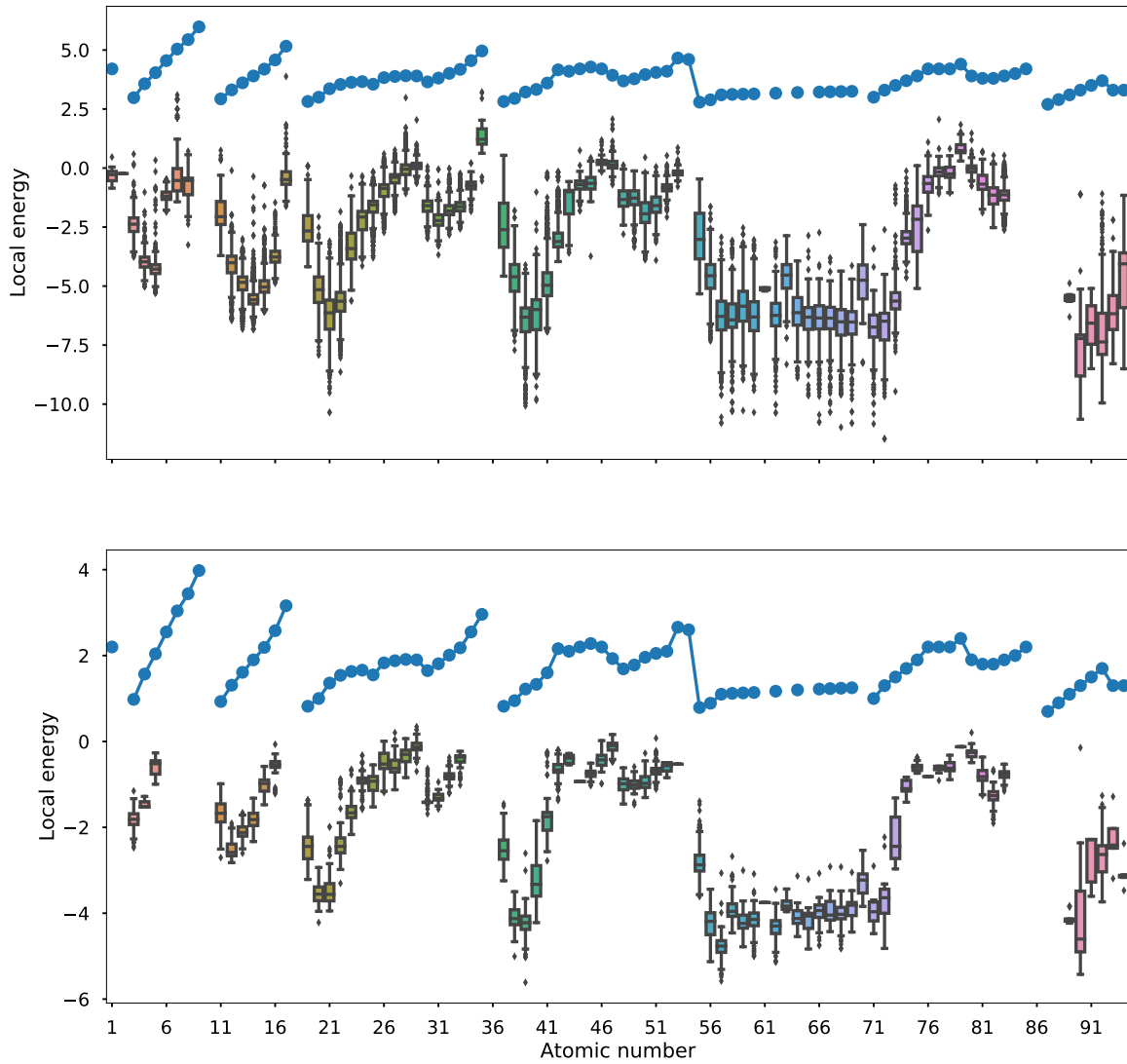


FIG. S3. The local energy of oxygen (upper) and sulfur (lower) coordination environments as a function of atomic number. The blue dotted line denotes the electronegativity of each element.